IEEE Access
Multidisciplinary | Rapid Review | Open Access Journal

Received 6 July 2022, accepted 28 July 2022, date of publication 1 August 2022, date of current version 5 August 2022.

Digital Object Identifier 10.1109/ACCESS.2022.3195930

RESEARCH ARTICLE

On the Performance and Optimization of HAPS Assisted Dual-Hop Hybrid RF/FSO System

RIMA DEKA[1], (Student Member, IEEE), VISHESH MISHRA[1], IMTIAZ AHMED[2], (Member, IEEE), SANYA ANEES[1], (Member, IEEE), AND MD. SAHABUL ALAM[3], (Member, IEEE)

[1]Indian Institute of Information Technology Guwahati, Guwahati 781015, India
[2]Howard University, Washington, DC 20059, USA
[3]California State University Northridge, Northridge, CA 91330, USA

Corresponding author: Imtiaz Ahmed (imtiaz.ahmed@howard.edu)

This work was supported in part by the Research Fund of DST Project ECR/2017/003367; and in part by the Start-Up Research Grant of the Department of Electrical Engineering and Computer Science, Howard University, Washington, DC, USA, (2018–2021).

ABSTRACT In this paper, we derive accurate outage probability and bit error rate expressions for a high altitude platform station (HAPS) assisted terrestrial communication system. In particular, HAPS is deployed as a relay node to assist two ground stations for data transmission. Each ground station-to-HAPS communication link works on a hybrid radio frequency (RF) and free space optics (FSO) mode. Selection combining is performed at the HAPS and the destination ground station to select either RF or FSO link based on the instantaneous channel signal-to-noise ratio (SNR). The accuracy of the derived outage probability and bit error rate expressions are validated with extensive computer simulations. We further develop an optimal power allocation scheme that optimizes the transmit power of source-ground-station and HAPS while satisfying practical energy consumption constraints. The derived expressions provide more insights on system design and assist analyzing HAPS-terrestrial integrated network supported by hybrid RF/FSO system.

INDEX TERMS High altitude platform station, free space optics communication, hybrid RF/FSO, outage probability, bit error rate, power allocation.

I. INTRODUCTION

Compared to radio frequency (RF) transmission, free space optics (FSO) communication has several advantages. FSO communications, for instance, can offer high transmission bandwidth, directivity, and security while operating on unlicensed spectrum and using less power. Despite these benefits, the FSO link's performance is frequently limited by air channel turbulence, which can cause beam scintillation and hence degrade the end-to-end system's performance [1], [2]. Furthermore, mechanical vibrations at the transceiver nodes cause the transmitter and receiver to become misaligned (known as *pointing error*). However, unlike FSO communication systems, RF communication technologies rarely encounter similar problems.

The associate editor coordinating the review of this manuscript and approving it for publication was Maurizio Magarini.

There have been numerous contributions in the literature to alleviate the constraints of FSO links. When RF technologies are used as a backup infrastructure for FSO communications, both communication systems complement each other and results in an efficient and robust system. The RF/FSO hybrid communication system has been shown to have a wide range of applications in a variety of communication networks, including ground-station satellite links, inter-satellite links, and so on. [3], [4]. Relay-assisted RF-FSO communication systems have also been proven to be an effective way to improve the performance of FSO links. [5]–[9], and [10] study the performance of mixed RF/FSO communication networks in various cooperative communication circumstances. An outage probability (OP) for a mixed RF/FSO amplify-and-forward (AF) communication system was calculated in [7] while considering M-distributed fading for the FSO link. Moreover, accurate error rate and OP expressions

were derived in [8] for an asymmetric dual hop fixed-gain AF cooperative RF/FSO system. The performance analysis framework developed in [8] was extended for decode-and-forward (DF) communication system in [9]. In [10], a switching scheme was proposed and the pertinent outage performance was analyzed for a hybrid RF/FSO DF cooperative communication network. The designed system operates in the FSO mode when the received signal-to-noise ratio (SNR) stays over a certain threshold SNR but switches back to the RF transmission mode when the SNR drops below the threshold value of SNR [11], [12].

Aerial communication systems [13] have been proposed by third generation partnership project (3GPP) in its release 17 to be adopted in cellular communication systems for fifth generation (5G) or beyond 5G (B5G) systems in order to provide an ad-hoc coverage to ensure the seamless or on-demand emergency communications [14]. Aerial networks can be configured with low altitude platform station/unmanned aerial vehicle (UAV) [15], [16] or high-altitude platform station (HAPS) [17]. In particular, HAPS has generated significant attention in recent years to provide connectivity services both in rural and urban areas and for achieving disaster-tolerant network applications [18]–[20]. Due to the unique properties of the stratosphere, HAPS can stay at a quasi-stationary position and can contribute significantly to the goal of ubiquitous connectivity [19]. HAPS is a quasi-stationary aerial platform that operates in stratosphere at an altitude mostly in the range of 18-21 km [18]. HAPS can be deployed both as aerial relays to enhance connectivity of terrestrial wireless systems and flying base stations to provide communication to the ground station users [21]–[23]. In general, HAPSs are deployed in the stratosphere in such a way so that the line-of-sight (LOS) link between the transmitter and the receiver is highly achievable [24], [25]. Therefore, the atmospheric turbulence, which is an inherent and unavoidable detrimental impact in FSO communications, has lower impact on HAPS.

Motivated by the combined advantages of HAPS and hybrid RF/FSO links, in this work, we consider the deployment of a HAPS as the relay node to assist terrestrial communication networks with hybrid RF/FSO systems [26]–[28] to enhance the network coverage as shown in Fig 1. The proposed design approach can be considered as a potential candidate for future integrated aerial-terrestrial networks in line with the B5G cellular communication paradigm [29]. In this regard, recently, a HAPS integrated hybrid RF/FSO communication system has been envisaged in [30], where the performance of a terrestrial-aerial-satellite uplink communication network has been investigated by developing end-to-end symbol error and system OP expressions.

In this article, we consider the integration of HAPS with existing terrestrial communication systems where the deployed HAPS will act as a DF [13], [31]–[33] relay node between the ground stations acting as the source and the destination. We considered DF approach to achieve considerable better performance than AF at low SNR. In particular, hybrid

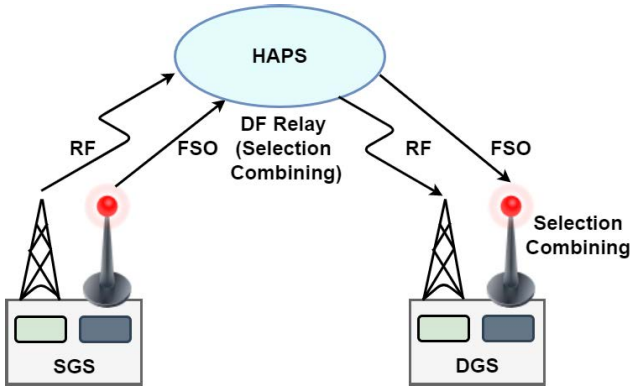

FIGURE 1. DF based dual hop Hybrid RF/FSO communication system for aerial-terrestrial integrated network.

RF/FSO communication systems [34], [35] are deployed in both the source-to-HAPS and the HAPS-to-destination links and selection combining (SC) scheme is applied at HAPS and destination node [36], [37]. FSO link has practical limitations like beam alignment, beam wander, scintillation, and changes caused by receiver's orientation deviations. The consequences of such degradation factors are considerable on long-range FSO links since they are dependent on the distance. As such, these factors are important to analyze the HAPS based FSO systems. In the previous works, researchers have used simple Gamma-Gamma channel model for characterizing the FSO channel which excludes the angle-of-arrival (AOA) fluctuations of the HAPS. In our study, we have considered the recent channel model [36] for HAPS based FSO propagation channel that incorporates all the possible factors, which may affect an FSO environment. To maintain the reliability of the system, we have used the RF link as a back-up for the considered system. Using hybrid link both at first ground station to HAPS and HAPS to second ground station provides new insights to our study. The performance of such system is analyzed in terms of OP and bit-error rate (BER). The analytical expressions are derived in terms of Meijer-G and Extended Bi-variate Meijer-G functions. In the numerical results, the dominating factors of the FSO link like beam width, instantaneous position fluctuation of the HAPS, atmospheric turbulence, and the shadowing parameters of the RF link are discussed. Furthermore to provide an insightful analysis, we have conducted the asymptotic analysis of the system. Moreover, the closed-form performance-indicator expressions are developed to design a power allocation algorithm to optimize the power of the transmitter and HAPS in our study. A similar model is considered in our previous work in [38], where some initial results are shown.

The contributions of this paper are summarized as follows:

- We propose and analyze a HAPS-assisted terrestrial communication system where each ground station-to-HAPS communication link works on a hybrid RF/FSO mode.

- To validate the performance of the proposed system, we derive an accurate system OP and BER expressions considering commonly used linear modulation techniques while leveraging the derived statistical characteristics of the instantaneous received SNR of the system.
- In addition, we derive the asymptotic BER and outage expressions that assist in rapid performance evaluation by providing insights into system design.
- We develop an optimal power allocation scheme by exploiting the derived closed-form OP expression. The proposed scheme jointly allocates the transmit power of the source-ground-station (SGS) and HAPS by minimizing the OP while satisfying practical energy consumption constraints.

From the obtained results, we demonstrate that the OP and the BER performances of the proposed system depends on different parameters, e.g., different RF fading parameters, different turbulence conditions of the FSO links, instantaneous position fluctuation of HAPS and the beam width of the transmitter, etc. Moreover, the asymptotic results truly resemble the derived analytical results for the sufficiently high SNR region. Simulation results reveal that the derived optimal power allocation scheme shows more than 3 dB SNR improvement over the equal power allocation scheme.

The rest of the paper is organized as follows. System and channel models are described in Sections II and III, respectively. The OP and error rate expressions are derived in Section IV. The statistical characteristics of system SNR is derived on Section V. The asymptotic analysis and optimal power allocation schemes are discussed in Section VI and VII, respectively. The analytical and simulation results of the considered system are shown in Section VIII, and the conclusions are made in Section IX.

II. SYSTEM MODEL

In this paper, we consider a HAPS assisted DF based dual-hop hybrid RF/FSO system, where an SGS communicates with the destination-ground-station (DGS) via HAPS (see Fig. 1). The overall data transmission is organized in two phases. The SGS communicates with the HAPS using a hybrid RF/FSO subsystem during the first phase, whereas the HAPS communicates with the DGS using another hybrid RF/FSO subsystem in the second hop. It is worth stating that SGS and DGS are assumed to be the components of a terrestrial communication network. However, we assume that the direct communication link between SGS and DGS is potentially hampered by blockage and strong shadowing effects. Therefore, HAPS works as a relay in DF mode between SGS and DGS nodes. The hybrid RF/FSO systems incorporate SC technique, which selects the signal with the best SNR at both HAPS and DGS. As HAPS works in DF mode, the signal with higher SNR in SGS-HAPS link is first decoded, then re-encoded and forwarded to DGS using the hybrid RF/FSO system. Like HAPS node, DGS selects the signal with higher SNR in HAPS-DGS link and decodes the signal.

The RF path for both SGS-HAPS and HAPS-DGS links are considered to follow Shadowed-Rician fading [30], whereas the FSO link is characterized by atmospheric attenuation, Gamma-Gamma (GG) distributed turbulence, Rayleigh distributed pointing errors, and the impacts of hovering fluctuations of the considered HAPS. It is worth mentioning that the position vibrations of the optical receiver as well as the AoA fluctuations of the received optical beam are lumped together in hovering fluctuations. Let us denote the received signal at HAPS transmitted by SGS via RF link as

$$y_{H,r} = h_1 x_S + n_H, \tag{1}$$

where h_1 represents the Shadowed-Rician distributed channel gain of the RF link and x_S denotes the signal transmitted by SGS. Furthermore, n_H is the complex valued additive white Gaussian noise (AWGN) with zero mean and variance $\sigma^2_{n,H}$. The instantaneous and average SNRs of SGS-HAPS RF link can be expressed as $\gamma_{rf_1} = \frac{P_{r_1}|h_1|^2}{\sigma^2_{n,H}}$ and $\Gamma_{rf_1} = \frac{P_{r_1}E[|h_1|^2]}{\sigma^2_{n,H}}$, respectively. Here, $E[\cdot]$ represents the expectation operator, $E[|h_1|]^2$ indicates the average power of LOS and non-line-of-sight (NLOS) or scattered components of the complex-valued channel gain, and P_{r_1} denotes the RF transmit power of SGS. Similar to RF, the received signal at HAPS transmitted by SGS via FSO link is given by

$$y_{H,f} = \eta_1 g_1 x_S + e_H, \tag{2}$$

where η_1 is the photo-electronic conversion ratio of the considered photo detector (PD) at HAPS, g_1 is the FSO channel co-efficient, and e_H is the complex valued AWGN with zero mean and variance $\sigma^2_{e,H}$. The instantaneous and average optical-equivalent electrical SNRs of the SGS-HAPS FSO link can be represented as $\gamma_{fso_1} = \frac{\eta_1^2 P_{t_1}|g_1|^2}{\sigma^2_{e,H}}$ and $\mu_{fso_1} = \frac{\eta_1^2 P_{t_1}E[|g_1|^2]}{\sigma^2_{e,H}}$, respectively, where P_{t_1} denotes the equivalent electrical transmit power of SGS node for FSO mode transmission.

On the other hand, in the second hop, the signal received at DGS originated from HAPS while passed through the RF link is given by

$$y_{D,r} = h_2 \hat{x}_S + n_D, \tag{3}$$

where h_2 represents the Shadowed-Rician distributed channel gain for the considered RF link and $\hat{x}_S$ denotes the detected signal at HAPS. We assume that HAPS node applies appropriate error correction coding scheme and hence ensures error-free detection. Therefore, we assume that $\hat{x}_S = x_S$. Moreover, n_D is the complex valued AWGN with zero mean and variance $\sigma^2_{n,D}$. The instantaneous and average SNRs of the HAPS-DGS RF link are denoted by $\gamma_{rf_2} = \frac{P_{r_2}|h_2|^2}{\sigma^2_{n,D}}$ and $\Gamma_{rf_2} = \frac{P_{r_2}E[|h_2|^2]}{\sigma^2_{n,D}}$, respectively, where P_{r_2} is the transmit power of HAPS. Again, the signal received at the DGS through HAPS-DGS FSO link is given by

$$y_{D,f} = \eta_2 g_2 \hat{x}_S + e_D, \tag{4}$$

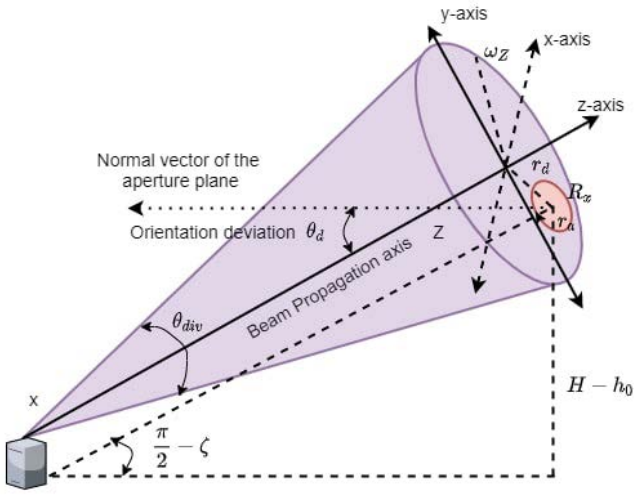

FIGURE 2. Schematic of optical uplink [41].

where η_2 is the photo-electronic conversion ratio of the considered PD at DGS, g_2 is the FSO channel co-efficient, and e_D is the AWGN with zero mean and variance $\sigma^2_{e,D}$.

The instantaneous and average optical-equivalent electrical SNRs of the (HAPS-DGS) FSO link are $\gamma_{fso_2} = \frac{\eta_2^2 P_{t_2} |g_2|^2}{\sigma^2_{e,D}}$ and $\mu_{fso_2} = \frac{\eta_2^2 P_{t_2} E[|g_2|^2]}{\sigma^2_{e,D}}$, respectively. Here, P_{t_2} represents the electrical equivalent transmit power of HAPS for FSO mode of data transmission. Finally, DGS performs SC and detects the signal transmitted from the HAPS.

III. CHANNEL MODELING

This section explains the considered channel models used for the RF and FSO links along with pertinent factors influencing the channel characteristics.

A. RF CHANNEL MODEL

In this work, we consider Shadowed-Rician distribution for both SGS-HAPS and HAPS-DGS links. This is a generalized RF fading channel model, which incorporates Rayleigh and Rician fading models as its special cases [30]. The probability density function (PDF) of the instantaneous SNR of the RF link γ_{rf_i}, $i \in \{1, 2\}$ is given by [30]

$$f_{\gamma_{rf_i}}(\gamma_{rf_i}) = \frac{\Omega P_i}{\Gamma_{rf_i}} \exp\left(-\frac{Q_i \Omega \gamma_{rf_i}}{\Gamma_{rf_i}}\right) F_1\left(m_1; 1; \frac{\Omega \delta_i \gamma_{rf_i}}{\Gamma_{rf_i}}\right), \quad (5)$$

where $\Omega = \Omega_i + 2b_i$, $P_i = \frac{\left(\frac{2b_i m_1}{2b_i m_i + \Omega_i}\right)^{m_i}}{2b_i}$, $Q_i = \frac{1}{2b_i}$, $\delta_i = \frac{0.5\Omega_i}{2b_i^2 m_i + b_i \Omega_i}$, $2b_i$ is the average power of the NLOS components, Ω_i is the average power of the LOS component, $0 \leq m_i \leq \infty$ is the Nakagami-m fading severity parameter, and $F_1(.;.;.)$ is the confluent hyper-geometric function [39]. The cumulative distribution function (CDF) of γ_{rf_i} using Kummer transformation [30], [40] is given by

$$F_{\gamma_{rf_i}}(\gamma_{rf_i}) = \sum_{k_i=0}^{m_i-1} \frac{\Omega P_i \psi}{((Q_i - \delta_i)\Omega)^{k_i+1}} \gamma\left(k_i+1, \frac{\Omega(Q_i-\delta_i)\gamma_{rf_i}}{\Gamma_{RF_i}}\right), \quad (6)$$

where $i \in \{1, 2\}$, $\psi = \frac{(m_i-1)!\delta_i^{k_1}\Omega_i^{k_1}}{(m_i-1-k_1)!(k_i!)^2}$, and $\gamma(.,.)$ represents the lower incomplete gamma function.

B. FSO CHANNEL MODEL

H. Safi [41] proposed an FSO channel model that incorporates four channel parameters into g_i namely attenuation loss g^i_{al}, atmospheric turbulence g^i_{at}, geometric loss g^i_{pl}, and AOA fluctuations g^i_{af}. We have considered simplex data transmission as a point to point communication for the considered two hops, where the source is connected to destination via a HAPS assisted DF relay, so the channel model for uplink and downlink are both characterized by Gamma-Gamma turbulence model. For uplink the turbulence condition is taken as mentioned in [41], whereas for downlink the turbulence model is taken as mentioned in the study [42], [43].We have considered the this model for both the links as it takes into account the receiver's position vibrations, pointing jitter variance induced by beam wander, detector aperture size, and received optical beam-width into account. Based on these defined parameters, the PDF of g_i, $i \in \{1, 2\}$ is given by [41]:

$$f_{g_i}(g_i) = \frac{2^{2C_{5_i}+1} C_{1_i}^{-C_{3_i}} g_i^{C_{3_i}-1} C_{4_i}}{(4\alpha_i\beta_i)^{C_{5_i}+1}} \Gamma\left(\frac{2C_{5_i}+2+\alpha_i-\beta_i}{2}\right) \times \Gamma\left(\frac{2C_{5_i}+2+\beta_i-\alpha_i}{2}\right)\left(1 - e^{\frac{-\theta^2_{FOV_i}}{2\sigma_o^2}}\right) + e^{\frac{-\theta^2_{FOV_i}}{2\sigma_o^2}} \delta(g_i). \quad (7)$$

Here, $C_{1_i} = 2(\frac{r_a}{\omega_Z})^2$, $C_{2_i} = 2/\omega_Z^2$, $C_{3_i} = \frac{1}{2C_{2_i}\sigma_r^2}$, $C_{4_i} = \frac{2C_{3_i}(\alpha_i\beta_i)^{\frac{\alpha_i+\beta_i}{2}}}{g_{al}^{C_3}\Gamma(\alpha_i)\Gamma(\beta_i)}$, and $C_{5_i} = \frac{\alpha_i+\beta_i-2C_{3_i}-2}{2}$. Moreover, $\Gamma(\cdot)$ is the Gamma function, $\delta(\cdot)$ represents the impulse function, r_a corresponds to radius of the receiver with variance σ_r^2, σ_o is the orientation deviation of the HAPS, and ω_Z denotes the beam waist at distance Z as shown in Fig. 2. Scalers α_i and β_i denote effective numbers of large scale and small scale eddies as per GG model for turbulence [41], and θ_{FOV_i} represents the angle of field of view (FOV).

Following (7), we obtain the PDF and the CDF of γ_{fso_i} as

$$f_{\gamma_{fso_i}}(\gamma_{fso_i}) = \frac{R_i^{C_{3_i}+1} \gamma_{fso_i}^{\frac{C_{3_i}-2}{2}}}{2(C_{3_i}+1)^{C_{3_i}} \mu_i^{\frac{C_{3_i}}{2}}} + \frac{R_i S_i \delta\left(\frac{R_i}{C_{3_i}+1}(\frac{\gamma_{fso_i}}{\mu_i})^{\frac{1}{2}}\right)}{2(C_{3_i}+1)(\mu_i\gamma_{fso_i})^{\frac{1}{2}}} \quad (8)$$

$$\text{and } F_{\gamma_{fso_i}}(\gamma_{fso_i}) = \frac{R_i^{C_{3_i}+1} \gamma_{fso_i}^{C_{3_i}/2}}{(C_{3_i}+1)^{C_{3_i}} C_{3_i} \mu_i^{C_{3_i}/2}} + S_i, \quad (9)$$

respectively. Here, $R_i = \frac{2^{2C_{5_i}+1} C_{1_i}^{-C_{3_i}} C_{4_i}}{(4\alpha_i\beta_i)^{C_{5_i}+1}} \Gamma\left(\frac{2C_{5_i}+2+\alpha_i-\beta_i}{2}\right) \times \Gamma\left(\frac{2C_{5_i}+2+\beta_i-\alpha_i}{2}\right)\left(1 - e^{\frac{-\theta^2_{FOV_i}}{2\sigma_o^2}}\right)$ and $S_i = e^{\frac{-\theta^2_{FOV_i}}{2\sigma_o^2}}$ for $i \in \{1, 2\}$.

IV. STATISTICAL CHARACTERISTICS OF THE SNR FOR HAPS ASSISTED HYBRID RF/FSO SYSTEM

As SC is used at the HAPS and the DGS to combine two received signals via RF and FSO links, the SNR of the signals received at HAPS and DGS individually is given by

$$\gamma_T = \max(\gamma_{rf_i}, \gamma_{fso_i}), \tag{10}$$

where $T \in \{SH, HD\}$, SH = source-to-HAPS, HD = HAPS-to-destination and $i \in \{1, 2\}$. Hence, the CDF of γ_T is given by

$$F_{\gamma_T}(\gamma) = F_{\gamma_{rf_i}}(\gamma) F_{\gamma_{fso_i}}(\gamma). \tag{11}$$

The end-to-end (SGS-HAPS-DGS) instantaneous SNR of the considered DF based dual-hop communication system can be stated as [9]

$$\gamma_e = \min(\gamma_{SH}, \gamma_{HD}). \tag{12}$$

Lemma 1: The CDF of γ_e can be represented by (15), as shown at the bottom of the page.

Proof: The CDF of γ_e can be expressed as

$$F_{\gamma_e}(\gamma) = 1 - (1 - F_{\gamma_{SH}}(\gamma))(1 - F_{\gamma_{HD}}(\gamma)). \tag{13}$$

Now by substituting (11) in (13), we can write the close form expression for system CDF in (14) as.

$$\begin{aligned} F_{\gamma_e}(\gamma) &= F_{\gamma_{rf_1}}(\gamma) F_{\gamma_{fso_1}}(\gamma) + F_{\gamma_{rf_2}}(\gamma) F_{\gamma_{fso_2}}(\gamma) \\ &\quad - F_{\gamma_{rf_1}}(\gamma) F_{\gamma_{fso_1}}(\gamma) F_{\gamma_{rf_2}}(\gamma) F_{\gamma_{fso_2}}(\gamma). \end{aligned} \tag{14}$$

Exploiting (6) and (9) in (14) results in (15), where $\xi_i = \frac{\Omega(Q_i - \delta_i)\gamma_e}{\Gamma_i}$. ■

Lemma 2: The PDF of γ for the considered system can be represented by (17), as shown at the bottom of the page.

Proof:

Differentiating (13) with respect to γ_e, the PDF of γ_e can be expressed as follows:

$$f_{\gamma_e}(\gamma) = f_{\gamma_{SH}}(\gamma) - f_{\gamma_{SH}}(\gamma) F_{\gamma_{HD}}(\gamma) + f_{\gamma_{HD}}(\gamma) - f_{\gamma_{HD}}(\gamma) F_{\gamma_{SH}}(\gamma), \tag{16}$$

where $f_{\gamma_{SH}}(\gamma) = f_{\gamma_{rf_1}} F_{\gamma_{fso_1}}(\gamma) + f_{\gamma_{fso_1}}(\gamma) F_{\gamma_{rf_1}}(\gamma)$ and $f_{\gamma_{HD}}(\gamma) = f_{\gamma_{rf_2}} F_{\gamma_{fso_2}}(\gamma) + f_{\gamma_{fso_2}}(\gamma) F_{\gamma_{rf_2}}(\gamma)$. Now by substituting (5), (8), and (11) in (15), we obtain (17). ■

Note that we exploit $F_{\gamma_e}(\gamma)$ and $f_{\gamma_e}(\gamma)$ depicted in Lemma 1 and 2, respectively to obtain the closed-form expressions of OP and BER for the considered HAPS assisted hybrid RF/FSO system in the Section V.

V. PERFORMANCE ANALYSIS

In this section, we derive the closed-form expressions of the OP and BER for the considered system that help the system designers to evaluate the performance of the considered systems while assisting in the design and the optimization of the communication nodes.

A. OUTAGE PROBABILITY (OP)

We define the OP of the considered HAPS assisted hybrid RF/FSO system as the probability of the event where the end-to-end instantaneous SNR γ falls below a predetermined threshold value γ_{th}. In particular, we represent the OP as $P_o = Pr[\gamma \leq \gamma_{th}]$, where $Pr[A]$ defines the probability of an event A. Following Lemmas 1 and 2 results in OP as represented by (18), as shown at the bottom of the next page.

B. BIT ERROR RATE (BER)

The BER of the considered system can be expressed using [44] as

$$P_e = \frac{v^u}{2\Gamma(u)} \int_0^\infty \gamma_e^{u-1} e^{-v\gamma_e} F_{\gamma_e}(\gamma) d\gamma, \tag{19}$$

where u and v are the modulation specific parameters representing different baseband modulation schemes as shown in Table 1. After substituting (14) in (17), P_e can be re-written as

$$F_{\gamma_e}(\gamma) = 1 - \prod_{i=1}^{2} \left(1 - \left(\frac{R_i^{C_{3_i}+1} \gamma^{\frac{C_{3_i}}{2}}}{(C_{3_i}+1)^{C_{3_i}} C_{3_i} \mu_1^{\frac{C_{3_i}}{2}}} + S_i\right) \times \left(\sum_{k_i=0}^{m_i-1} \frac{\Omega P_i \psi}{((Q_i - \delta_i)\Omega)^{k_i+1}} \gamma\left(k_i + 1, \xi_i\right)\right)\right). \tag{15}$$

$$\begin{aligned} f_{\gamma_e}(\gamma) &= \sum_{i=1}^{2} \Bigg[\frac{\Omega P_i}{\Gamma_{RF_i}} e^{-\frac{Q_i \Omega \gamma}{\Gamma_{RF_i}}} F_1(m_1; 1; \frac{\Omega \delta_i \gamma}{\Gamma_{RF_i}}) \left(\frac{R_i^{C_{3_i}+1} \gamma^{\frac{C_{3_i}}{2}}}{(C_{3_i}+1)^{C_{3_i}} C_{3_i} \mu_{fso_i}^{\frac{C_{3_i}}{2}}} + S_i \right) + \left(\frac{R_i^{C_{3_i}+1} \gamma^{\frac{C_{3_i}-2}{2}}}{2(C_{3_i}+1)^{C_{3_i}} \mu_{fso_i}^{\frac{C_{3_i}}{2}}} + \frac{R_i S_i \delta(\frac{R_i}{C_{3_i}+1} (\frac{\gamma}{\Gamma_{fso_i}})^{\frac{1}{2}})}{2(C_{3_i}+1)(\Gamma_{fso_i}\gamma)^{\frac{1}{2}}} \right) \\ &\quad \times \sum_{k_i=0}^{m_i-1} \frac{\Omega P_i \psi}{((Q_i - \delta_i)\Omega)^{k_i+1}} \times \gamma\left(k_i+1, \frac{\Omega(Q_i - \delta_i)\gamma}{\Gamma_{RF_i}}\right) \Bigg[1 - \left(\frac{R_i^{C_{3_i}+1} \gamma^{\frac{C_{3_i}}{2}}}{(C_{3_i}+1)^{C_{3_i}} C_{3_i} \mu_2^{\frac{C_{3_i}}{2}}} + S_i \right) \left(\sum_{j_i=0}^{m_{3-i}-1} \frac{\Omega P_{3-i} \psi}{((Q_{3-i} - \delta_{3-i})\Omega)^{j_i+1}} \gamma\left(j_i+1, \xi_{3-i}\right) \right) \Bigg]. \end{aligned} \tag{17}$$

TABLE 1. BER parameters for various modulation techniques [24].

Binary Modulation techniques	u	v
Coherent binary frequency shift keying (CBFSK)	0.5	0.5
Coherent binary phase shift keying (CBPSK)	0.5	1
Non-coherent binary frequency shift keying (NBFSK)	1	0.5
Differential binary phase shift keying (DBPSK)	1	1

$$P_e = \frac{v^u}{2\Gamma(u)} \int_0^\infty \gamma_e^{u-1} e^{-v\gamma_e} [F_{\gamma_{rf_1}}(\gamma) F_{\gamma_{fso_1}}(\gamma) + F_{\gamma_{rf_2}}(\gamma) \times F_{\gamma_{fso_2}}(\gamma) - F_{\gamma_{rf_1}}(\gamma) F_{\gamma_{fso_1}}(\gamma) F_{\gamma_{rf_2}}(\gamma) F_{\gamma_{fso_2}}(\gamma)] d\gamma. \tag{20}$$

P_e can be further expressed in a simplified form as

$$P_e = I_1 + I_2 - I_3, \tag{21}$$

where I_1, I_2, and I_3 are expressed as follows:

$$I_i = \frac{v^u}{2\Gamma(u)} \int_0^\infty \gamma_e^{u-1} e^{-v\gamma_e} F_{\gamma_{rf_i}}(\gamma) F_{\gamma_{fso_i}}(\gamma) d\gamma, \tag{22}$$

where $i \epsilon \{1, 2, 3\}$.

Combining (6) and (9) in above equation I_i can be re-written as

$$I_j = \frac{v^u}{2\Gamma(u)} \int_0^\infty \gamma^{u-1} e^{-v\gamma} \Bigg[\Bigg(\frac{R_i^{C_{3_i}+1} \gamma^{\frac{C_{3_i}}{2}}}{(C_{3_i}+1)^{C_{3_i}} C_{3_i} \mu_1^{\frac{C_{3_i}}{2}}} \Bigg) \times \Bigg(\sum_{k_i=0}^{m_i-1} \frac{\Omega P_i \psi}{((Q_i - \delta_i)\Omega)^{k_{2i-1}+1}} \gamma\Big(k_i + 1, \xi_i\Big) \Bigg) \Bigg) + S_i \Bigg(\sum_{k_i=0}^{m_i-1} \frac{\Omega P_i \psi}{((Q_i - \delta_i)\Omega)^{k_{2i-1}+1}} \gamma\Big(k_i + 1, \xi_i\Big) \Bigg) \Bigg) \Bigg] d\gamma, \tag{23}$$

where $j \in \{1, 2\}$ and,

$$I_3 = \frac{v^u}{2\Gamma(u)} \int_0^\infty \gamma^{u-1} e^{-v\gamma} F_{\gamma_{rf_1}}(\gamma) F_{\gamma_{fso_1}}(\gamma) \times F_{\gamma_{rf_2}}(\gamma) F_{\gamma_{fso_2}}(\gamma) d\gamma. \tag{24}$$

After substituting (6) and (9) in (20), I_3 can be written as

$$I_3 = \frac{v^u}{2\Gamma(u)} \int_0^\infty \gamma^{u-1} e^{-v\gamma} \Bigg[\prod_{i=1}^{2} \Bigg(\frac{R_i^{C_{3_i}+1} \gamma^{C_{3_i}/2}}{(C_{3_i}+1)^{C_{3_i}} C_{3_i} \mu_1^{\frac{C_{3_i}}{2}}} \Bigg) \times \Bigg(\sum_{k_i=0}^{m_i-1} \frac{\Omega P_i \psi}{((Q_i - \delta_i)\Omega)^{k_i+1}} \gamma\Big(k_i + 1, \xi_i\Big) \Bigg) + \sum_{i=1}^{2} S_i \Bigg(\sum_{k_i=0}^{m_i-1} \frac{\Omega P_i \psi}{((Q_i - \delta_i)\Omega)^{k_i+1}} \gamma\Big(k_i + 1, \xi_i\Big) \Bigg) \times \Bigg(\frac{R_i^{C_{3_i}+1} \gamma^{C_{3_i}/2}}{(C_{3_i}+1)^{C_{3_i}} C_{3_i} \mu_1^{C_{3_i}/2}} \Bigg) \Bigg(\sum_{k_i=0}^{m_i-1} \frac{\Omega P_i \psi}{((Q_i - \delta_i)\Omega)^{k_i+1}} \times \gamma\Big(k_i + 1, \xi_i\Big) \Bigg) + \prod_{i=1}^{2} S_i \Bigg(\sum_{k_i=0}^{m_i-1} \frac{\Omega P_i \psi}{((Q_i - \delta_i)\Omega)^{k_i+1}} \times \gamma\Big(k_i + 1, \xi_i\Big) \Bigg) \Bigg] d\gamma. \tag{25}$$

I_j in (23) can be further simplified by converting exponential and lower incomplete gamma function into their equivalent Meijer-G function by exploiting $e^{-x} = G_{0,1}^{1,0}\Big(x \Big| \begin{matrix} - \\ 0 \end{matrix}\Big)$, $\gamma(\alpha, x) = G_{1,2}^{1,1}\Big(x \Big| \begin{matrix} 1 \\ \alpha, 0 \end{matrix}\Big)$ and then utilizing [45, Eq 07.34.21.0011.01], as

$$I_j = \frac{A_i v^{\frac{-C_{3_i}}{2}} R_i^{C_{3_i}+1} G_{2,2}^{1,2}\Big[\Big(\frac{\xi_1}{v}\Big) \Big| \begin{matrix} 1, (1-u-\frac{C_{3_i}}{2}) \\ k_1+1, 0 \end{matrix}\Big]}{2\Gamma(u) C_{3_i} (C_{3_i}+1)^{C_{3_i}} \mu_i^{\frac{C_{3_i}}{2}}} + \frac{A_i S_i}{2\Gamma(u)} G_{2,2}^{1,2}\Big[\Big(\frac{\xi_1}{v}\Big) \Big| \begin{matrix} 1, (1-u) \\ k_1+1, 0 \end{matrix}\Big], \tag{26}$$

where $A_j = \sum_{k_1=0}^{m_i-1} \frac{\Omega P_i \psi}{((Q_i - \delta_i)\Omega)^{k_i+1}}$ and $G_{p,q}^{m,n}[.]$ is the Meijer's G-function as defined in [45].

Moreover, I_3 can be further expressed as

$$I_3 = L_1 + L_2 + L_3 + L_4, \tag{27}$$

where

$$L_1 = \frac{v^u}{2\Gamma(u)} \int_0^\infty \gamma^{u-1} e^{-v\gamma} \prod_{i=1}^{2} \Bigg(\frac{R_i^{C_{3_i}+1} \gamma^{C_{3_i}/2}}{(C_{3_i}+1)^{C_{3_i}} C_{3_i} \mu_1^{\frac{C_{3_i}}{2}}} \Bigg) \times \Bigg(\sum_{k_i=0}^{m_i-1} \frac{\Omega P_i \psi}{((Q_i - \delta_i)\Omega)^{k_i+1}} \gamma\Big(k_i + 1, \xi_i\Big) \Bigg) \Bigg) d\gamma, \tag{28}$$

$$L_2 = \frac{v^u}{2\Gamma(u)} \int_0^\infty \gamma^{u-1} e^{-v\gamma} \Bigg(\frac{R_1^{C_{3_1}+1} \gamma^{C_{3_1}/2}}{(C_{3_1}+1)^{C_{3_1}} C_{3_1} \mu_1^{\frac{C_{3_1}}{2}}} \Bigg) \times \Bigg(\sum_{k_1=0}^{m_1-1} \frac{\Omega P_1 \psi}{((Q_1 - \delta_1)\Omega)^{k_1+1}} \gamma\Big(k_1 + 1, \xi_i\Big) \Bigg) \times S_2 \Bigg(\sum_{k_2=0}^{m_2-1} \frac{\Omega P_2 \psi}{((Q_2 - \delta_2)\Omega)^{k_2+1}} \gamma\Big(k_2 + 1, \xi_i\Big) \Bigg) d\gamma, \tag{29}$$

$$P_o = 1 - \prod_{i=1}^{2} \Bigg(1 - \Bigg(\frac{R_i^{C_{3_i}+1} \gamma_{th}^{C_{3_i}/2}}{(C_{3_i}+1)^{C_{3_i}} C_{3_i} \mu_1^{C_{3_i}/2}} + S_i \Bigg) \times \Bigg(\sum_{k_i=0}^{m_i-1} \frac{\Omega P_i \psi}{((Q_i - \delta_i)\Omega)^{k_{2i-1}+1}} \gamma\Big(k_{2i-1} + 1, \frac{\Omega(Q_i - \delta_i)\gamma_{th}}{\Gamma_i}\Big) \Bigg) \Bigg). \tag{18}$$

$$L_3 = \frac{v^u}{2\Gamma(u)} \int_0^\infty \gamma^{u-1} e^{-v\gamma} \left(\frac{R_2^{C_{3_2}+1} \gamma^{C_{3_2}/2}}{(C_{3_2}+1)^{C_{3_2}} C_{3_2} \mu_1^{\frac{C_{3_2}}{2}}} \right) \times \left(\sum_{k_1=0}^{m_1-1} \frac{\Omega P_1 \psi}{((Q_1-\delta_1)\Omega)^{k_1+1}} \gamma\left(k_1+1, \xi_i\right) \right) \times S_1 \left(\sum_{k_1=0}^{m_1-1} \frac{\Omega P_1 \psi}{((Q_1-\delta_2)\Omega)^{k_1+1}} \gamma\left(k_1+1, \xi_i\right) \right) d\gamma, \tag{30}$$

and,

$$L_4 = \frac{v^u}{2\Gamma(u)} \int_0^\infty \gamma^{u-1} e^{-v\gamma} S_1 \left(\sum_{k_1=0}^{m_1-1} \frac{\Omega P_1 \psi}{((Q_1-\delta_2)\Omega)^{k_1+1}} \gamma \times \left(k_1+1, \xi_i\right) \right) S_2 \left(\sum_{k_2=0}^{m_2-1} \frac{\Omega P_2 \psi}{((Q_2-\delta_2)\Omega)^{k_2+1}} \gamma\left(k_2+1, \xi_i\right) \right) d\gamma. \tag{31}$$

Further simplifications of L_1 can be accomplished by converting exponential and lower incomplete gamma function into its equivalent Meijer-G function by using $e^{-x} = G_{0,1}^{1,0}\left(x \middle| \begin{matrix} - \\ 0 \end{matrix}\right)$, $\gamma(\alpha, x) = G_{1,2}^{1,1}\left(x \middle| \begin{matrix} 1 \\ \alpha, 0 \end{matrix}\right)$. This approach will incorporate three Meijer-G functions i.e., one for exponential function and others for two lower incomplete gamma function. Then by leveraging [45, Eq 07.34.21.0081.01], we can write L_1 in the form of extended generalized bi-variate Meijer G-function. The final expression of L_1 is given by (32), as shown at the bottom of the next page. Following the similar approach, L_2, L_3 and L_4 lead to (33), (34), and (35), as shown at the bottom of the next page. Here, $G_{q,p:p_1,q_1:p_2,q_2}^{n,m:m_1,n_1:m_2,n_2}[.|.|.|.]$ represnts the extended generalized bi-variate Meijer G-function [44]. The closed-form expression for BER of the considered system can be obtained by substituting (26) and (27) in (21).

VI. ASYMPTOTIC ANALYSIS

In this section, the asymptotic expressions for OP and BER are derived in closed-form for the considered hybrid RF/FSO dual-hop systems. Note that these expressions provide more insights on the system design. The asymptotic outage probability expression for the dual-hop hybrid FSO/RF HAPS system when $\Gamma_i \to \infty$ is given by

$$P_o^{asy} = F_{\gamma_e}^{asy}(\gamma_{th}), \tag{36}$$

Here, the asymptotic expression for CDF of the considered system is obtained by converting lower incomplete gamma function into its equivalent Meijer-G function using $\gamma(\alpha, x) = G_{1,2}^{1,1}\left(x \middle| \begin{matrix} 1 \\ \alpha, 0 \end{matrix}\right)$ and thereby applying [45, Eq eq.(07.34.06.0040.01)] in (15) as follows:

$$F_{\gamma_e}^{asy}(\gamma) = 1 - \prod_{i=1}^{2} \left(1 - \left(\frac{R_i^{C_{3_i}+1} \gamma^{lC_{3_i}/2}}{(C_{3_i}+1)^{C_{3_i}} C_{3_i} \mu_i^{C_{3_i}/2}} + \zeta_i \right) \times \left(\sum_{k_i=0}^{m_i-1} \frac{\Omega P_i \psi}{((Q_i-\delta_i)\Omega)^{k_i+1}} \times \zeta_i^{k_i+1} \times \frac{\Gamma[1+k_i]}{1+k_i} \right) \right). \tag{37}$$

The asymptotic BER expression can be obtained by putting asymptotic CDF i.e., (37) in (19) as [8], [44]

$$P_e^{asy} = \frac{v_u}{2\Gamma[u]} \int_0^\infty \gamma^{u-1} e^{-v\gamma} F_\gamma^{asy}(\gamma_e) d\gamma = \sum_{i=1}^{8} B_i, \tag{38}$$

where

$$B_1 = \frac{v_u}{2\Gamma[u]} \int_0^\infty \gamma^{u-1} e^{-v\gamma} P' \gamma^{C_{3_2}/2} d\gamma = \frac{v_u P'}{2\Gamma[u]} \left(\frac{1}{v}\right)^{u+\frac{C_{3_2}}{2}+k_2+1} \Gamma[u + \frac{C_{3_2}}{2} + k_2 + 1] \times \frac{1}{k_2+1}, \tag{39}$$

$$B_2 = \frac{v_u}{2\Gamma[u]} \int_0^\infty \gamma^{v+k_2-1} e^{-v\gamma} S_2 Z' d\gamma = \frac{v_u S_2 Z'}{2\Gamma[u]} \left(\frac{1}{v}\right)^{v+k_2+1} \Gamma[u+k_2+1] \times \frac{1}{k_2+1}, \tag{40}$$

$$B_3 = \frac{v_u}{2\Gamma[u]} \int_0^\infty xZ \gamma^{u+k_1+1-1} e^{-v\gamma} \gamma^{C_{3_1}/2} d\gamma = \frac{v_u xZ}{2\Gamma[u]} \left(\frac{1}{v}\right)^{u+\frac{C_{3_1}}{2}+k_1+1} \Gamma[u + \frac{C_{3_1}}{2} + k_1 + 1] \times \frac{1}{k_1+1}, \tag{41}$$

$$B_4 = \frac{v_u}{2\Gamma[u]} \int_0^\infty \gamma^{M-1} xZ \times x'Z' e^{-v\gamma} d\gamma = \frac{v_u xZx'Z'}{2\Gamma[u]} \left(\frac{1}{v}\right)^{M} \Gamma[M] \times \frac{1}{(k_1+1)(k_2+1}, \tag{42}$$

$$B_5 = \frac{v_u}{2\Gamma[u]} \int_0^\infty \gamma^{M-1} xZy'Z' e^{-v\gamma} d\gamma = \frac{v_u xZy'Z'}{2\Gamma[u]} \left(\frac{1}{v}\right)^{M} \Gamma[M] \times \frac{1}{(k_1+1)(k_2+1}, \tag{43}$$

$$B_6 = \frac{v_u}{2\Gamma[u]} \int_0^\infty yZ \gamma^{u+k_1+1-1} e^{-v\gamma} d\gamma = \frac{v_u yZ}{2\Gamma[u]} \left(\frac{1}{v}\right)^{u+k_1+1} \Gamma[u+k_1+1] \times \frac{1}{k_1+1}, \tag{44}$$

$$B_7 = \frac{v_u}{2\Gamma[u]} \int_0^\infty \gamma^{M-1} x'Z'yZ e^{-v\gamma} d\gamma = \frac{v_u x'Z'yZ}{2\Gamma[u]} \left(\frac{1}{v}\right)^{M} \Gamma[M] \times \frac{1}{(k_1+1)(k_2+1}, \tag{45}$$

and

$$B_8 = \frac{v_u}{2\Gamma[u]}\int_0^\infty \gamma^{M-1} xyZy'Z' e^{-v\gamma} d\gamma = \frac{v_u yZy'Z'}{2\Gamma[u]}\left(\frac{1}{v}\right)^M \Gamma[M] \times \frac{1}{(k_1+1)(k_2+1}. \quad (46)$$

In $B_k, k \in \{1,2\}$, $x = \frac{R_1^{C_{3_1}+1}\gamma^{C_{3_1}/2}}{(C_{3_1}+1)^{C_{3_1}} C_{3_1} \mu_1^{C_{3_1}}}$, $y = S_1$, $x'_D = \frac{R_2^{C_{3_2}+1}\gamma^{C_{3_2}/2}}{(C_{3_2}+1)^{C_{3_2}} C_{3_1} \mu_1^{C_{3_2}}}$, $y' = S_2$, $Z = \sum_{k_1=0}^{m_1-1} \frac{\Omega P_1 \psi \Gamma[k_1+1]}{((Q_1-\delta_1)\Omega)^{k_1+1}} \times \zeta_x^{k_1+1}$, $\zeta_x = \frac{(Q_i-\delta_i)\Omega}{\Gamma_1}$, $Z' = \sum_{k_2=0}^{m_2-1} \frac{\Omega P_1 \psi \Gamma[k_2+1]}{((Q_2-\delta_2)\Omega)^{k_2+1}} \times \zeta_y^{k_2+1}$, $\zeta_y = \frac{(Q_i-\delta_i)\Omega}{\Gamma_2}$, and $M = u + \frac{C_{3_1}}{2} + \frac{C_{3_1}}{2} + k_1 + k_2 + 2$.

VII. OPTIMAL POWER ALLOCATION FOR HAPS AIDED RF-FSO SYSTEM

In this section, we exploit the derived closed-form performance-indicator expressions to develop an optimal power allocation (OPA) algorithm that jointly optimizes the transmit power of SGS and HAPS while satisfying individual and total power constraints. The developed power allocation framework is general enough to incorporate per node or network-wide power budgets depending on the system requirements. Our objective is to formulate an optimization framework while leveraging the derived OP expression and thereby solve the problem in polynomial time so that the solution algorithm can compute optimal transmit powers for SGS and HAPS in real-time data transmission. We assume SGS is the central node[1] of the hybrid RF/FSO network that collects all the pertinent information and statistics from HAPS and DGS through the control channel to calculate the derived OP in (36). Once collected, SGS applies the OPA scheme, calculates the optimal transmit powers (of RF and FSO links) for itself (SGS) and HAPS, and then broadcasts this information (optimal transmit power) prior to data transmission.

[1]HAPS and DGS can run OPA scheme as well in the considered system model.

A. PROBLEM FORMULATION FOR OPA

In particular, we minimize the derived asymptotic OP P_o^{asy} in (36) by optimally allocating RF and (electrical equivalent) FSO transmit powers of both SGS and HAPS. We formulate an optimization problem as follows:

$$\min_{[P_{r_1}, P_{t_1}, P_{r_2}, P_{t_2}] \succcurlyeq 0} \quad P_o^{asy} \quad (47)$$

$$s.t. \quad P_{r_1} \le E_{r_1}, \quad (48)$$

$$P_{t_1} \le E_{t_1}, \quad (49)$$

$$P_{r_2} \le E_{r_2}, \quad (50)$$

$$P_{t_2} \le E_{t_2}, \quad (51)$$

$$P_{r_1} + P_{t_1} \le E_1, \quad (52)$$

$$P_{r_2} + P_{t_2} \le E_2, \quad (53)$$

$$P_{r_1} + P_{t_1} + P_{r_2} + P_{t_2} \le E_T, \quad (54)$$

where E_{r_1}, E_{t_1}, E_{r_2}, and E_{t_2} represent the maximum power budget for RF transmitter at SGS, FSO transmitter at SGS, RF transmitter at HAPS, and FSO transmitter at HAPS, respectively. Moreover, E_1, E_2, and E_T denote the total maximum power budget at SGS, total maximum power budget at HAPS, and total power budget for SGS and HAPS, respectively. It is worth mentioning that the solution of problem (47)-(54) results in optimal transmit power of RF and FSO transmitters for SGS and HAPS, i.e., $P_{r_1}^*$, $P_{r_2}^*$, $P_{t_1}^*$, and $P_{t_2}^*$.

B. SOLUTION APPROACH FOR OPA

Note that objective function (47) and constraints (52)–(54) can be classified as posynomials, whereas constraints (48)–(51) are regarded as monomials [46], [47]. Therefore, the optimization problem defined in (47)-(54) can be classified as a geometric program [46]. It is worth pointing that any geometric program can be converted into an equivalent convex optimization problem by applying logarithmic transformation via change of variables [48]. Once transformed, the equivalent convex optimization problem can be solved optimally and in polynomial time complexity using well-defined and robust algorithms, e.g., interior-point method, gradient-descent approach, etc. [48]. We leveraged

$$L_1 = \frac{q^{-C_{3_1}} A_1 A_2}{2\Gamma(u)} \left(\frac{R_1^{C_{3_1}+1}}{(C_{3_1}+1)^{C_{3_1}} C_{3_1} \mu_1^{C_{3_1}/2}}\right)\left(\frac{R_2^{C_{3_2}+1}}{(C_{3_2}+1)^{C_{3_2}} C_{3_2} \mu_2^{C_{3_2}/2}}\right) \times G_{1,0:1,2:1,2}^{0,1:1,1:1,1}\left[\begin{matrix}\left(\frac{\xi_1}{v}\right) \\ \left(\frac{\xi_2}{v}\right)\end{matrix}\middle| \begin{matrix}1-u-c_3 \\ .\end{matrix}\middle| \begin{matrix}1 \\ k_1+1, 0\end{matrix}\middle| \begin{matrix}1 \\ k_2+1, 0\end{matrix}\right] \quad (32)$$

$$L_2 = \frac{v^{\frac{-C_{3_1}}{2}} A_1 A_2}{2\Gamma(u)} \left(\frac{R_1^{C_{3_1}+1}}{(C_{3_1}+1)^{C_{3_1}} C_{3_1} \mu_1^{C_{3_1}/2}} S_2\right) \times G_{1,0:1,2:1,2}^{0,1:1,1:1,1}\left[\begin{matrix}\left(\frac{\xi_1}{v}\right) \\ \left(\frac{\xi_2}{v}\right)\end{matrix}\middle| \begin{matrix}1-u-0.5c_3 \\ .\end{matrix}\middle| \begin{matrix}1 \\ k_2+1, 0\end{matrix}\middle| \begin{matrix}1 \\ k_2+1, 0\end{matrix}\right]. \quad (33)$$

$$L_3 = \frac{v^{\frac{-C_{3_2}}{2}} A_1 A_2}{2\Gamma(u)} \left(\frac{R_2^{C_{3_2}+1}}{(C_{3_2}+1)^{C_{3_2}} C_{3_2} \mu_2^{C_{3_2}/2}} S_1\right) \times G_{1,0:1,2:1,2}^{0,1:1,1:1,1}\left[\begin{matrix}\left(\frac{\xi_1}{v}\right) \\ \left(\frac{\xi_2}{v}\right)\end{matrix}\middle| \begin{matrix}1-u-0.5c_3 \\ .\end{matrix}\middle| \begin{matrix}1 \\ k_1+1, 0\end{matrix}\middle| \begin{matrix}1 \\ k_2+1, 0\end{matrix}\right]. \quad (34)$$

$$L_4 = \frac{A_1 A_2}{2\Gamma(u)} S_1 S_2 \times G_{1,0:1,2:1,2}^{0,1:1,1:1,1}\left[\begin{matrix}\left(\frac{\xi_1}{v}\right) \\ \left(\frac{\xi_2}{v}\right)\end{matrix}\middle| \begin{matrix}1-u \\ .\end{matrix}\middle| \begin{matrix}1 \\ k_1+1, 0\end{matrix}\middle| \begin{matrix}1 \\ k_2+1, 0\end{matrix}\right]. \quad (35)$$

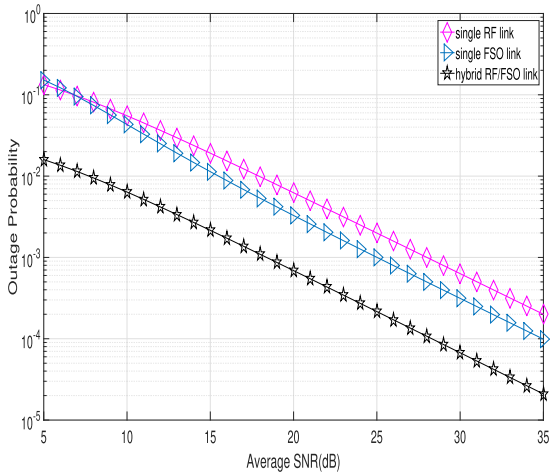

FIGURE 3. OP vs. average SNR for single FSO, RF and hybrid RF/FSO system.

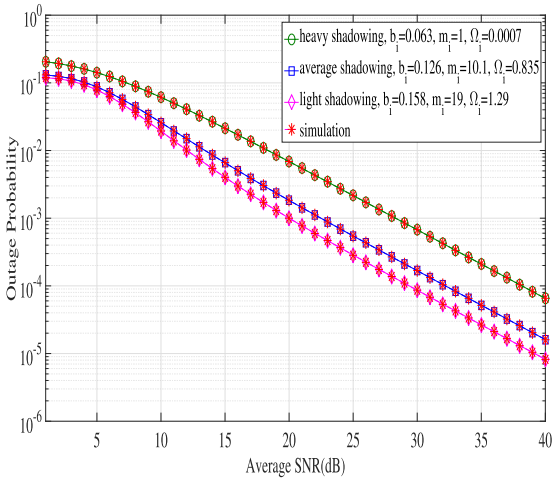

FIGURE 4. OP vs. average SNR for different RF shadowing parameter.

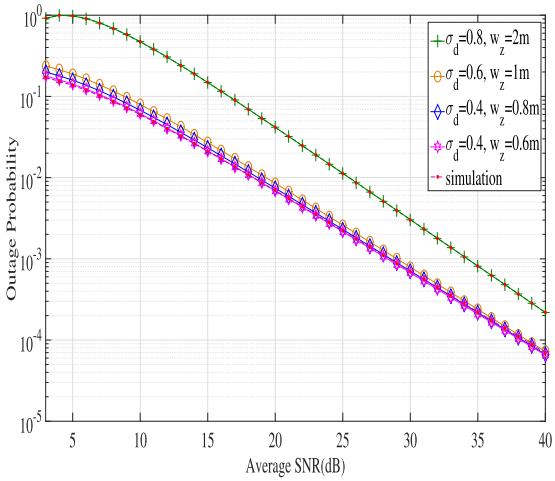

FIGURE 5. OP vs. average SNR for different values of angle of deviation σ_d and beam width ω_z.

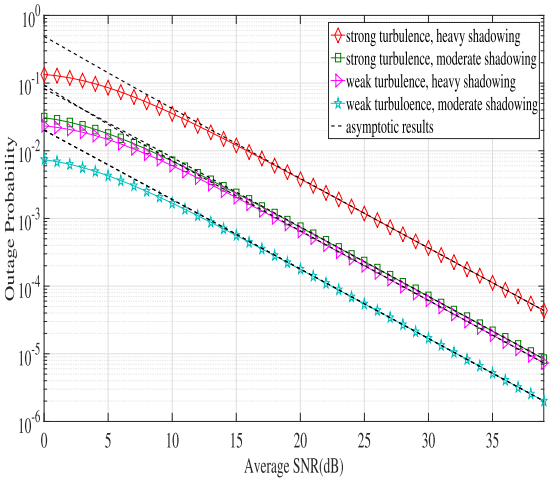

FIGURE 6. Asymptotic analysis for OP as a function of average SNR.

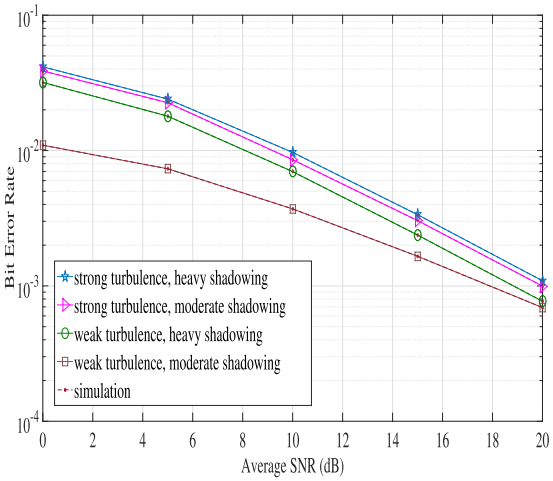

FIGURE 7. BER vs. average SNR for both strong and moderate turbulence condition and different shadowing parameters.

open-source tool, CVX on MATLAB platform [49] to solve the geometric program for the proposed OPA scheme in Section VIII. The optimal transmit powers can be calculated once in every coherence-time or once in the order of multiple coherence-time intervals depending on the system requirements. It is worth mentioning that the defined optimization problem represents a large class of power allocation problems by adopting different values of E_{r_1}, E_{t_1}, E_{r_2}, E_{t_2}, E_1, E_2, and E_T. For instance, if SGS and HAPS have enough sources of energy, E_{r_1}, E_{t_1}, E_{r_2}, E_{t_2}, E_1, and E_2 possess very high values and thereby constraints (48)–(53) can be discarded from optimization problem (47)-(54). On the other hand, if SGS and HAPS are designed to operate independently, constraint (54) can be removed from the optimized framework.

VIII. NUMERICAL RESULTS

In this section, the analytical expressions derived in the previous section for HAPS assisted dual-hop hybrid RF/FSO communication system are evaluated and validated by Monte Carlo simulations. In MATLAB, there are 10^6 samples used per simulation to generate the simulated results.The system performance is evaluated in terms of systems OP and BER. In particular, we study the impact of different system parameters e.g., RF fading, FSO fading, angle of deviation, beam

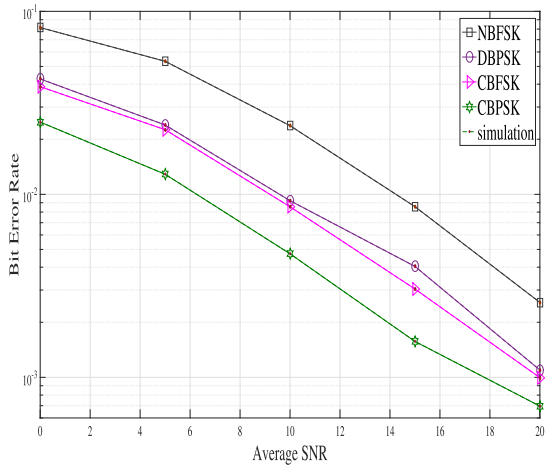

FIGURE 8. BER vs. average SNR for different modulation schemes.

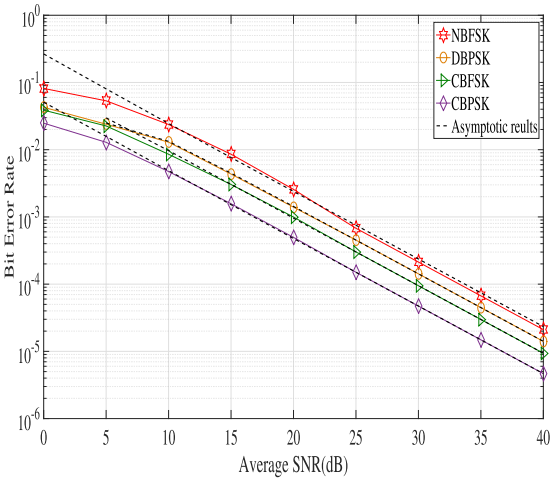

FIGURE 9. Asymptotic BER as a function of average SNR.

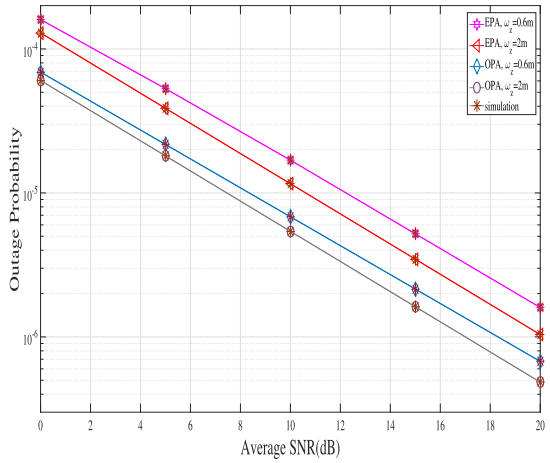

FIGURE 10. OP vs. average SNR for optimal and equal power allocation schemes. OPA and EPA stand for optimal power allocation and equal power allocation, respectively.

width, etc. on outage and error rate performances in this section. Here, we set the variance of AOA $\sigma_o = 16$ mrad, the beam width at the transmitter $\omega_z = 0.6$ m, the instantaneous position fluctuation of the HAPS $\sigma_d = 0.4$, the FOV of the receiver $\theta_{FOV} = 75$ mrad and $\Omega_z = 0.6$m for producing

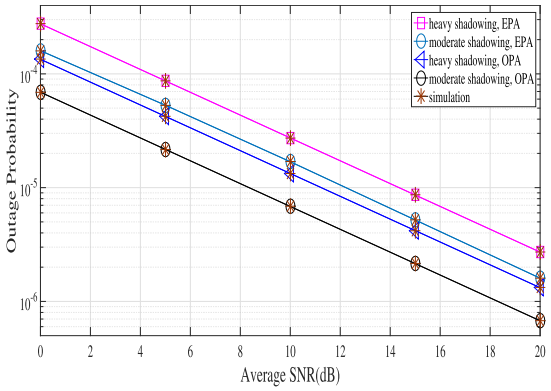

FIGURE 11. OP vs. average SNR for optimal and equal power allocation schemes with different shadowing parameters.

different numerical results, as the link performance is sensitive to the amount of the receiver FOV. For given AOA, we considered the optimal value of FOV to achieve minimum outage and BER for a given orientation deviation. Moreover, we set the aperture radius of the FSO system, $r_a = 5$ cm, the orientation deviation, $\sigma_0 = 15$ mrad and the link length, $Z = 20$ km.

In Fig. 3, the OP vs. average SNR is plotted for single RF, single FSO, and the hybrid RF/FSO system. In this figure, our objective is to compare the performances among different configurations of RF and FSO links. Here, we observe that the hybrid system results in a better performance compared to the single RF or FSO schemes over the entire range of considered SNR. The objective of this comparison is to demonstrate the effectiveness of hybrid RF/FSO system.

In Fig. 4, the OP of the considered HAPS associated hybrid RF/FSO system for different RF fading parameters are evaluated. All the simulated results confirm the theoretical outcomes over the considered range of average SNR. In this figure, we have considered strong turbulence condition for the FSO signal for both SGS-HAPS and HAPS-DGS links. Precisely, we set $\alpha_i = 4.2$ and $\beta_i = 1.4$. We consider three scenarios of RF fading by changing b_i, m_i, and ω_i, $i \in \{1, 2\}$. It is evident from Fig. 4 that the system is in more outage when we consider the heavy shadowing as compared to the average and light shadowing. It is worth pointing out that in case of heavy shadowing, the presence of multi-path components are more prominent than the presence of the LOS component.

Fig. 5 shows OP vs. average SNR while considering different FSO channel parameters, i.e., instantaneous position fluctuation of HAPS σ_d and the beam width of the transmitter ω_z. The atmospheric turbulence for FSO signal is considered to be strong ($\alpha = 4.2$ and $\beta = 1.4$) and the RF signal undergoes heavy shadowing ($b_i = 0.063$, $m_i = 1$ and $\Omega_i = 0.0007$) in this case. From Fig. 5, it is evident that the OP of the system increases when the instantaneous position fluctuations of the HAPS increases. The figure shows that the OP of the system also depends on ω_z, and increasing ω_z does not necessarily decrease the system outage. Moreover, we observe from Fig. 5 that the effect of beam wander on

the OP is significant at low SNR. For example, in case of 10 dB SNR, the outage probabilities of the system are 5.97×10^{-2}, 6.76×10^{-2}, 7.95×10^{-2}, and 4.7×10^{-1} for $(\sigma_d, \omega_z) = (0.4, 0.6)$, $(0.4, 0.8)$, $(0.6, 1)$, and $(0.8, 2)$, respectively.

In Fig. 6, we validate the developed asymptotic expressions for OP for sufficiently high average SNRs. It is worth pointing out that the asymptotic expressions of OP and BER assist the system designers for more intuitive analysis. In Fig. 6, we have obtained the asymptotic results for OP by varying different RF fading parameters and FSO turbulence parameters. Moreover, it is evident from the figure that at high SNR the asymptotic results match with the analytical results.

Fig. 7 shows the BER vs. average SNR of the considered HAPS associated hybrid RF/FSO system for different atmospheric turbulence conditions of the FSO systems and different shadowing parameters of RF links for both SGS-HAPS and HAPS-DGS links. For all the considered cases in this figure, we have incorporated the moderate and heavy shadowing effects for the RF link. It is observed from Fig. 7 that the system yields a better performance in case of weak turbulence as compared to the strong atmospheric turbulence while considering moderate shadowing effect.

Fig. 8 shows the BER vs. average SNR of the considered HAPS associated hybrid RF/FSO system for different binary modulation schemes e.g. CBFSK, CBPSK, DBPSK, and NBFSK. Recall that u and v in Table.1 represent the modulation specific parameters. In this figure, we have considered the moderate shadowing effect for the RF link and strong atmospheric turbulence for the FSO link. It is evident from the figure that CBPSK yields the lowest BER amongst all the considered modulation schemes.

In Fig. 9, the asymptotic results for BER of the considered system is obtained for different binary modulation schemes. The FSO turbulence parameter is considered to be strong and RF fading is considered to be heavy shadowing. It is observed from the figure that the system shows better performance while considering CBPSK modulation scheme. Moreover, the asymptotic result match with the analytical for high average SNR values.

We show the effectiveness of the proposed OPA scheme developed in Section VII in Figs. 10 and 11 by demonstrating the OP (calculated based on optimized transmit powers) as a function of average SNR. In particular, we compare the performance of the OPA scheme with equal power allocation (EPA), which is adopted as a baseline scheme for the considered system. In EPA, we set equal transmit powers for RF and FSO links for SGS and HAPS nodes without applying any optimization scheme. Our objective is to show a practical application of the derived performance analysis tools (e.g., OP expression) and thereby to demonstrate the advantages of OPA scheme in optimizing the system performance. For the considered use-case, we assume that the total power budget is 7 W. In particular, we set $E_{t1} = 0.0149$ W and $E_{t2} = 0.0117$ W for the FSO links and $E_{r1} = 3.8981$ W and $E_{r2} = 3.0753$ W for the RF links while evaluating OPA scheme. While considering the EPA scheme we assume that the total power budget is 7 W as well (to accurately compare OPA with EPA) and hence we allocate equal power to the all links, i.e., $E_{t1} = E_{t2} = E_{r1} = E_{r2} = 1.75$ W. In Fig. 10, we have obtained the results for both OPA and EPA by varying the beamwidth at the transmitter ω_z. Moreover, the strong turbulence for FSO links and heavy shadowing for the RF links are assumed for the considered use cases. In case of Fig 11, the OP for OPA and EPA is obtained by varying the RF shadowing parameters. The FSO turbulence parameters are considered to be strong in this case. We observe that for all the considered use cases, OPA scheme yields lower OP as compared to EPA over the considered range of SNR. Also, we achieve more than 3dB gain with the developed OPA scheme over the baseline EPA scheme. These findings demonstrate the effectiveness of the proposed OPA for different use cases and make it a strong candidate for power allocation in the considered hybrid RF/FSO system. As described in Section VII, the proposed OPA scheme requires a geometric program to solve [46] and the program can be solved in polynomial time complexity, the proposed power allocation scheme can be readily implemented in real-time data transmission.[2]

IX. CONCLUSION

HAPS has generated significant attention in recent years to improve the connectivity services in terrestrial networks. In this article, we have presented the mathematical model to verify the OP and BER performances of a HAPS assisted dual-hop hybrid RF/FSO communication network, where HAPS works in the DF mode to assist two ground stations of the terrestrial network. We also investigated the optimal power allocation scheme for the proposed model. SC is performed at HAPS and DGS to select the better communication link (in between RF and FSO link) that yields better local channel state information. While deriving the OP and BER expressions, we obtained closed-form expressions of the PDF and the CDF of the end-to-end instantaneous channel SNRs for the considered system. Simulation results confirm the accuracy of the proposed analytical results. From the obtained results, it is observed that the OP and the bit error rate (BER) performances of the proposed system depends on different parameters, like different RF fading parameters, different turbulence conditions of the FSO links, instantaneous position fluctuation of HAPS, and the beam width of the transmitter, etc. Moreover, the asymptotic results truly resembles the derived analytical results for the high SNR region. Additionally, the derived optimal power allocation scheme shows more than 3 dB SNR improvement over the baseline equal power allocation scheme.

[2]For instance, the proposed optimization approach is applicable in fourth generation (4G) long-term evolution (LTE) or 5G new radio (NR) communication systems, where the transmission time interval (TTI) for resource block allocations are in the order of milliseconds.

REFERENCES

[1] X. Zhu and J. M. Kahn, "Free-space optical communication through atmospheric turbulence channels," *IEEE Trans. Commun.*, vol. 50, no. 8, pp. 1293–1300, Aug. 2002.

[2] M. A. Khalighi and M. Uysal, "Survey on free space optical communication: A communication theory perspective," *IEEE Commun. Surveys Tuts.*, vol. 16, no. 4, pp. 2231–2258, 4th Quart., 2014.

[3] M. Najafi, V. Jamali, and R. Schober, "Optimal relay selection for the parallel hybrid RF/FSO relay channel: Non-buffer-aided and buffer-aided designs," *IEEE Trans. Commun.*, vol. 65, no. 7, pp. 2794–2810, Jul. 2017.

[4] N. D. Chatzidiamantis, G. K. Karagiannidis, E. E. Kriezis, and M. Matthaiou, "Diversity combining in hybrid RF/FSO systems with PSK modulation," in *Proc. IEEE Int. Conf. Commun. (ICC)*, Jun. 2011, pp. 1–6.

[5] E. Lee, J. Park, D. Han, and G. Yoon, "Performance analysis of the asymmetric dual-hop relay transmission with mixed RF/FSO links," *IEEE Photon. Technol. Lett.*, vol. 23, no. 21, pp. 1642–1644, Nov. 1, 2011.

[6] I. S. Ansari, F. Yilmaz, and M.-S. Alouini, "Impact of pointing errors on the performance of mixed RF/FSO dual-hop transmission systems," *IEEE Wireless Commun. Lett.*, vol. 2, no. 3, pp. 351–354, Jun. 2013.

[7] H. Samimi and M. Uysal, "End-to-end performance of mixed RF/FSO transmission systems," *IEEE/OSA J. Opt. Commun. Netw.*, vol. 5, no. 11, pp. 1139–1144, Nov. 2013.

[8] S. Anees and M. R. Bhatnagar, "Performance of an amplify-and-forward dual-hop asymmetric RF–FSO communication system," *IEEE/OSA J. Opt. Commun. Netw.*, vol. 7, no. 2, pp. 124–135, Feb. 2015.

[9] S. Anees and M. R. Bhatnagar, "Performance evaluation of decode-and-forward dual-hop asymmetric radio frequency-free space optical communication system," *IET Optoelectron.*, vol. 9, no. 5, pp. 232–240, Oct. 2015.

[10] S. Sharma, A. S. Madhukumar, and R. Swaminathan, "Switching-based cooperative decode-and-forward relaying for hybrid FSO/RF networks," *IEEE/OSA J. Opt. Commun. Netw.*, vol. 11, no. 6, pp. 267–281, Jun. 2019.

[11] M. Sharma, D. Chadha, and V. Chandra, "High-altitude platform for free-space optical communication: Performance evaluation and reliability analysis," *J. Opt. Commun. Netw.*, vol. 8, no. 8, pp. 600–609, 2016.

[12] O. B. Yahia, G. K. Kurt, E. Erdoğan, and I. Altunbas, "A weather-dependent hybrid RF/FSO satellite communication for improved power efficiency," Tech. Rep., Jul. 2021.

[13] S. S. Sarma, R. Hazra, and P. H. J. Chong, "Performance analysis of DF relay assisted D2D communication in 5G mm-wave network," Tech. Rep., 2022.

[14] *3GPP: UAS-UAV*. [Online]. Available: https://www.3gpp.org/uas-uav

[15] A. Upadhya, "Investigation of mixed RF/FSO decode-and-forward NOMA cooperative relaying networks," *Wireless Pers. Commun.*, vol. 124, pp. 2923–2938, Feb. 2022.

[16] L. Qu, G. Xu, Z. Zeng, N. Zhang, and Q. Zhang, "UAV-assisted RF/FSO relay system for space-air-ground integrated network: A performance analysis," *IEEE Trans. Wireless Commun.*, early access, Feb. 8, 2022, doi: 10.1109/TWC.2022.3147823.

[17] O. B. Yahia, E. Erdogan, G. K. Kurt, I. Altunbas, and H. Yanikomeroglu, "HAPS selection for hybrid RF/FSO satellite networks," *IEEE Trans. Aerosp. Electron. Syst.*, early access, Jan. 11, 2022, doi: 10.1109/TAES.2022.3142116.

[18] M. S. Alam, G. K. Kurt, H. Yanikomeroglu, P. Zhu, and N. D. Dao, "High altitude platform station based super macro base station constellations," *IEEE Commun. Mag.*, vol. 59, no. 1, pp. 103–109, Jan. 2021.

[19] G. Karabulut Kurt, M. G. Khoshkholgh, S. Alfattani, A. Ibrahim, T. S. J. Darwish, M. S. Alam, H. Yanikomeroglu, and A. Yongacoglu, "A vision and framework for the high altitude platform station (HAPS) networks of the future," *IEEE Commun. Surveys Tuts.*, vol. 23, no. 2, pp. 729–779, 2nd Quart., 2021.

[20] S. Dutta, F. Hsieh, and F. W. Vook, "HAPS based communication using mmWave bands," in *Proc. IEEE Int. Conf. Commun. (ICC)*, May 2019, pp. 1–6.

[21] F. Fidler, M. Knapek, J. Horwath, and W. R. Leeb, "Optical communications for high-altitude platforms," *IEEE J. Sel. Topics Quantum Electron.*, vol. 16, no. 5, pp. 1058–1070, Oct. 2010.

[22] M. Alzenad, M. Z. Shakir, H. Yanikomeroglu, and M.-S. Alouini, "FSO-based vertical backhaul/fronthaul framework for 5G+ wireless networks," *IEEE Commun. Mag.*, vol. 56, no. 1, pp. 218–224, Jan. 2018.

[23] X. Cao, P. Yang, M. Alzenad, X. Xi, D. Wu, and H. Yanikomeroglu, "Airborne communication networks: A survey," *IEEE J. Sel. Areas Commun.*, vol. 36, no. 10, pp. 1907–1926, Sep. 2018.

[24] M. Q. Vu, T. V. Pham, N. T. Dang, and A. T. Pham, "Outage performance of HAP-UAV FSO links with Gaussian beam and UAV hovering," in *Proc. IEEE 92nd Veh. Technol. Conf. (VTC-Fall)*, Nov. 2020, pp. 1–5.

[25] E. Erdogan, I. Altunbas, G. K. Kurt, and H. Yanikomeroglu, "Cooperation in space: HAPS-aided optical inter-satellite connectivity with opportunistic scheduling," *IEEE Commun. Lett.*, vol. 26, no. 4, pp. 882–886, Apr. 2022.

[26] M. Jin, W. Liu, Y. Hao, R. Wu, Z. Wei, D. Deng, and H. Liu, "Hybrid dual-hop RF/FSO terrestrial-deep space communication system under solar scintillation during superior solar conjunction," *Appl. Sci.*, vol. 12, no. 2, p. 619, Jan. 2022.

[27] M. Torabi, N. Mohammadi, and C. Nerguizian, "Performance analysis of an asymmetric two-hop amplify-and-forward relaying RF–FSO system in a cognitive radio with partial relay selection," *Opt. Commun.*, vol. 505, Feb. 2022, Art. no. 127478.

[28] H. Wang, Z. Zhang, B. Zhu, and Y. Zhang, "Performance analysis of hybrid RF-reconfigurable intelligent surfaces assisted FSO communication," 2022, *arXiv:2201.08563*.

[29] J. Liu, Y. Shi, Z. M. Fadlullah, and N. Kato, "Space-air-ground integrated network: A survey," *IEEE Commun. Surveys Tuts.*, vol. 20, no. 4, pp. 2714–2741, 4th Quart., 2018.

[30] S. R, S. Sharma, N. Vishwakarma, and A. S. Madhukumar, "HAPS-based relaying for integrated space–air–ground networks with hybrid FSO/RF communication: A performance analysis," *IEEE Trans. Aerosp. Electron. Syst.*, vol. 57, no. 3, pp. 1581–1599, Jun. 2021.

[31] A. Girdher, A. Bansal, and A. Dubey, "On the performance of SLIPT-enabled DF relay-aided hybrid OW/RF network," *IEEE Syst. J.*, early access, Jan. 4, 2022, doi: 10.1109/JSYST.2021.3135957.

[32] H. A. Siddig, A. M. Salhab, and S. A. Zummo, "Performance analysis and optimization of multiuser mixed FSO/RF cognitive radio DF relay network," *Arabian J. Sci. Eng.*, vol. 47, pp. 3649–3657, Feb. 2022.

[33] R. Deka and S. Anees, "Performance analysis of a Decode-and-forward based mixed RF-FSO-VLC system," Tech. Rep., 2022.

[34] S. K. Shrivastava, S. Sengar, and S. P. Singh, "Effect of pointing error on the performance of improved modified switching scheme of hybrid FSO/RF system under mixture gamma atmospheric turbulence," *IETE J. Res.*, pp. 1–13, Jan. 2022.

[35] J. Ding, X. Xie, L. Tan, J. Ma, and D. Kang, "Dual-hop RF/FSO systems over κ-μ shadowed and Fisher-snedecor F fading channels with non-zero boresight pointing errors," *J. Lightw. Technol.*, vol. 40, no. 3, pp. 708–719, Feb. 1, 2022.

[36] H. Safi, A. Dargahi, J. Cheng, and M. Safari, "Analytical channel model and link design optimization for ground-to-HAP free-space optical communications," *J. Lightw. Technol.*, vol. 38, no. 18, pp. 5036–5047, Sep. 15, 2020.

[37] O. B. Yahia, E. Erdogan, and G. K. Kurt, "On the performance of HAPS-assisted hybrid RF-FSO multicast communication systems," Tech. Rep., 2021.

[38] R. Deka, V. Mishra, I. Ahmed, S. Anees, and M. S. Alam, "Performance analysis of HAPS assisted dual-hop hybrid RF/FSO system," in *Proc. IEEE 94th Veh. Technol. Conf. (VTC-Fall)*, Sep. 2021, pp. 1–5.

[39] M. T. Dabiri, S. M. S. Sadough, and M. A. Khalighi, "FSO channel estimation for OOK modulation with APD receiver over atmospheric turbulence and pointing errors," *Opt. Commun.*, vol. 402, pp. 577–584, Nov. 2017.

[40] S. Riechelmann, M. Schrempf, and G. Seckmeyer, "Simultaneous measurement of spectral sky radiance by a non-scanning multidirectional spectroradiometer (MUDIS)," *Meas. Sci. Technol.*, vol. 24, no. 12, Dec. 2013, Art. no. 125501.

[41] H. Safi, A. Dargahi, J. Cheng, and M. Safari, "Analytical channel model and link design optimization for ground-to-HAP free-space optical communications," *J. Lightw. Technol.*, vol. 38, no. 18, pp. 5036–5047, Sep. 15, 2020.

[42] L. T. S. Y. J. Ma, K. Li, and Y. Cao, "Performance analysis of satellite-to-ground downlink coherent optical communications with spatial diversity over gamma–gamma atmospheric turbulence," *Appl. Opics*, vol. 54, no. 25, pp. 7575–7585, 2015.

[43] R. L. P. L. C. Andrews, *Laser Beam Propagation through Random Media*, 2nd ed. Bellingham, WA, USA: SPIE, 2005.

[44] I. S. Ansari, S. Al-Ahmadi, F. Yilmaz, M. S. Alouini, and H. Yanikomeroglu, "A new formula for the BER of binary modulations with dual-branch selection over generalized-K composite fading channels," *IEEE Trans. Commun.*, vol. 59, no. 10, pp. 2654–2658, Oct. 2011.

[45] *Mathematica*, Wolfram Research, Champaign, IL, USA.

[46] S. Boyd, S.-J. Kim, L. Vandenberghe, and A. Hassibi, "A tutorial on geometric programming," *Optim. Eng.*, vol. 8, no. 1, pp. 67–127, Mar. 2007.
[47] M. Chiang, C. W. Tan, D. P. Palomar, D. O'Neill, and D. Julian, "Power control by geometric programming," *IEEE Trans. Wireless Commun.*, vol. 6, no. 7, pp. 2640–2651, Jul. 2007.
[48] S. Boyd, S. P. Boyd, and L. Vandenberghe, *Convex Optimization*. Cambridge, U.K.: Cambridge Univ. Press, 2004.
[49] M. Grant and S. Boyd. (Mar. 2014). *CVX: MATLAB Software for Disciplined Convex Programming, Version 2.1*. [Online]. Available: http://cvxr.com/cvx

RIMA DEKA (Student Member, IEEE) received the Bachelor of Technology degree in electronics and communication engineering from North Eastern Hill University, Meghalaya, India, in 2013, and the master's degree in technology from Assam Don Bosco University, India, in 2016. Currently, she is working as a Ph.D. Scholar with the Department of Electronics and Communication Engineering, Indian Institute of Information Technology Guwahati, Assam, India. Her research interests include optical wireless communications and cooperative communications. In her master's degree, she has been awarded University Gold Medal (2014–2016) for being University Topper in Electronics and Communication Engineering Branch.

VISHESH MISHRA is currently pursuing the B.Tech. degree in electronics and communication engineering with the Indian Institute of Information Technology Guwahati. His research interests include optical wireless communications and cooperative communications. He also works in the domain of power-aware computer architecture, approximate computing, and fault tolerance.

IMTIAZ AHMED (Member, IEEE) received the Ph.D. degree in electrical and computer engineering from the University of British Columbia, Vancouver, BC, Canada. He is currently an Assistant Professor with the Department of Electrical Engineering and Computer Science, Howard University, Washington, DC, USA. He works in the areas of wireless communications, signal processing, and computer networks. After finishing his Ph.D. degree, he worked at Intel Corporation, San Diego, CA, USA, as a Wireless Systems Engineer and Marshall University, Huntington, WV, USA, as an Assistant Professor. Currently, he is working on artificial intelligence aided physical layer design, integration of aerial and terrestrial communication networks, and communication with energy harvesting nodes.

SANYA ANEES (Member, IEEE) received the master's degree (W/D) in communication engineering from The University of Manchester, U.K., and the Ph.D. degree from the Indian Institute of Technology Delhi. She is currently an Assistant Professor with the Department of Electronics and Communication Engineering, Indian Institute of Information Technology Guwahati, India. Her research interests include optical wireless communications, HAPS-based aerial communications, MIMO systems, and cooperative communications. She has been awarded Early Career Research Award by SERB, India. In her graduation, she has been awarded University Gold Medal, in 2010, Shri Rawatpura Sarkar Gold Medal, in 2010, and Prof. S. T. Chakravati Gold Medal, in 2010, for being University Topper.

MD. SAHABUL ALAM (Member, IEEE) received the Ph.D. degree in electrical engineering from the Ecole de Technologie Superieure (ETS), Montreal, QC, Canada. He is currently an Assistant Professor with the Department of Electrical and Computer Engineering, California State University Northridge (CSUN), Northridge, CA, USA. He awarded the Governor General of Canada Gold Medal for Ph.D. degree. After finished his Ph.D.degree, he worked as a Postdoctoral Fellow with the Systems and Computer Engineering Department, Carleton University, with Prestigious Canadian Government FRQNT Fellowship. His current research interests include aerial communications with more focus on high altitude platform station (HAPS)-based communications, integration of terrestrial and non-terrestrial communications, reliable wireless communications in impulsive channel, cooperative communications, smart grid communications, NOMA, and massive MIMO for terrestrial and aerial communications.